**Proceedings of the ASME 2024 43rd International Conference on Ocean, Offshore and Arctic Engineering**
**OMAE2024**
**June 9-14, 2024, Singapore EXPO, Singapore**

**OMAE2024-123555**

# WAVE LOADS ON A HOLLOW CIRCULAR CYLINDER IN OPEN AND ICY WATERS

**Hongtao Li [1,*], Ersegun Deniz Gedikli[2], Zhengshun Cheng[3], Junji Sawamura[1], Raed Lubbad [4]**

[1]Osaka University, Osaka, Japan
[2]University of Hawai'i at Mānoa, Honolulu, Hawaii, United States
[3]Shanghai Jiao Tong University, Shanghai, China
[4]Norwegian University of Science and Technology, Trondheim, Norway

## ABSTRACT

*Arctic offshore structures are subject to combined wave-ice actions. However, the underlying mechanisms governing the interaction between waves, ice, and these structures remain inadequately understood. Performing well-controlled laboratory experiments is a fundamental approach to acquiring insights into such complicated physical processes.*

*This paper builds on analyzing the laboratory data that were obtained from the HYDRALAB+ Transnational Access project: Loads on Structure and Waves in Ice (LS-WICE), and studies the inline wave forces on a model-scale, stationary, vertical, semi-submerged, bottomless circular cylindrical shell structure, both with and without the presence of ice. In the experiment, the structure was exposed to unidirectional monochromatic waves with increasing heights at prescribed periods under open-water and ice-infested conditions. In the latter case, the ice field comprised uniformly sized and densely packed rectangular ice floes.*

*Various data analysis techniques, including Prony, dynamic mode decomposition, fast Fourier transform, Tikhonov regularization-based denoising, and Singular Spectrum Analysis, are applied to obtain a reliable estimate of wave amplitudes and the magnitudes of wave loads.*

*The experimental results suggest that the wave loads on the hollow cylinder, when surrounded by a fragmented ice cover, decrease by up to 27% in comparison to the ice-free water condition. This reduction results primarily from the attenuation of waves in an ice field.*

**Keywords: Wave Loads, Ice, Hollow Cylinder, LS-WICE**

## 1. INTRODUCTION

With the continuously growing need for energy, more offshore infrastructures such as oil platforms and wind turbines are expected to be installed inside the Arctic Circle [1] and in ice-covered regions, e.g., Baltic Sea [2]. In addition, there is an increase in shipping activities in the Arctic due to shrinking ice extent [3, 4]. Structures situated or sailing in ice-prone seawater experience the combined wave and ice loads. Under severe polar conditions, several structures in icy waters were damaged [5, 6].

To mitigate the risk of human life and economic loss and polluting the fragile environment in the Arctic, a fundamental understanding of the mechanisms that induce extreme loads on these structures deployed in Arctic and Sub-Arctic regions requires experiments conducted in idealized laboratory settings.

Previous laboratory studies principally focus on ice loads on these structures in still water, e.g. Refs. [7, 8]. There are very few experimental investigations of the loads on offshore structures that are simultaneously exposed to wave forcing and ice impact. Ref. [9] examined loads on a hexagonal cylinder that advanced in an ice field composed of synthetic ice floes under wave actions. Ref. [10] studied how ice loads on model ship change in waves compared to those in the still water covered by circular ice floes, which were modeled by polypropylene plate.

To the best of the authors' knowledge, no refrigerated ice has been used to study the change of wave loads on a structure between an ice-infested situation and ice-free water. A transnational laboratory experiment performed in 2016 using lab-grown saline ice provides a unique dataset to bridge this gap. By exploring this dataset, Ref. [11] presented a preliminary analysis of wave loads on an open-bottom cylinder in a broken ice field. In this study, we perform an extensive comparative analysis of wave loads on the hollow cylinder with/without the presence of ice. A variety of methods, together with Singular Spectrum Analysis (SSA, Refs. [12, 13]) that for the first time was applied to a polar engineering problem, was employed to analyze the measurements collected to attain a reliable estimate of wave load amplitudes.

The rest of this paper is structured in the following way. Section 2 describes the experimental setup. Section 3 presents several measurement analysis techniques. Section 4 demonstrates

*Corresponding author: Hongtao_Li@naoe.eng.osaka-u.ac.jp

the application of these data techniques to estimate wave amplitudes. Section 5 compares recorded wave loads in open water with those identified by data analysis methods from measured total inline loads in icy water. Section 6 concludes the present study with major findings.

## 2. EXPERIMENTS

The experimental tests described here were part of the Hydralab+ project: Loads on Structure and Waves in Ice (LS-WICE) under the EU Horizon 2020 programme for research and innovation [14, 15], and were carried out in the Large Ice Model Basin (length × width × depth = $72\,m \times 10\,m \times 2.5\,m$) of Hamburg Ship Model Basin (HSVA) in Germany.

Figure 1 shows the experimental setup for test series #4000 (ice-covered) and #5000 (open-water). In the ice basin, four flap-type wave makers were installed on one side, while a wooden parabolic-shaped beach was deployed on the opposite side to absorb incident waves. Along the lateral tank wall, twelve underwater pressure sensors with different separations were placed to measure wave elevations. Their distance from the wall was around $0.65\,m$. Among them, pressure sensors P11 and P12 collocated but were immersed at different depths. A vertical, bottomless, fixed, model-size, hollow circular cylinder, with its main particulars being provided in Table 1, positioned at $x = 43.7\,m$, $y = 4.3\,m$. Loads on the hollow cylinder were measured by a force transducer that attached this structure to the carriage. On a cantilever beam hanging over the hollow cylinder, two ultrasound sensors together with a GoPro camera were mounted (Fig. 2). The ultrasound sensors monitored wave runup, while the camera obliquely facing towards the cylinder documented near-field fluid-structure (test series #5000) and wave-ice-structure interactions (test series #4000).

**TABLE 1:** GEOMETRIC DIMENSIONS OF THE MODEL-SCALE, RESTRAINED HOLLOW CYLINDER

| | | | |
|---|---|---|---|
| Outer radius | $b$ | [m] | 0.343 |
| Inner radius | $a$ | [m] | 0.340 |
| Height | $H_c$ | [m] | 0.625 |
| Draft | $D$ | [m] | 0.360 |

In test series #4000, a saline level ice sheet grew overnight to $3.3\pm0.2\,cm$ thick and was cut into rectangular ice floes of identical size ($L_x \times L_y = 1.5\,m \times 1.63\,m$) from $x = 20\,m$ up to $51\,m$ in the following day. From $x = 51\,m$ onwards, the remaining ice sheet was intact and leaned against the damping beach (Fig. 1b). To study the dynamics of ice floes under wave actions, ice-ice, and ice-structure collisions, an upstream ice floe beside the cylinder was instrumented with an inertial measurement unit (IMU), as shown in Fig. 2b.

To systematically compare the wave loads on the hollow cylinder in open water with those in a fragmented ice field, regular incident waves with the same set of periods ($T$) and heights ($H$) were generated in test series #4000 (icy water) and #5000 (open water). As shown in Table 2, wave periods changed from 1.5 to $2\,s$, and heights increased from $0.025\,m$ to $0.100\,m$. The last column lists the values of the parameter $\sqrt{ka}$, where $k$ and $a$ are wavenumber in open water and the internal radius of the cylinder, respectively.

Test runs #4340 and #4430 are not analyzed here. This is because the upstream neighboring ice floe broke during the preceding test run #4330, which would certainly affect the near-field hydrodynamics (see Fig. 3 in comparison to Fig. 2b). The failure of the ice floe is caused by the combined loads from the impact with the cylinder and cyclic wave forcing. The whole fracture process happened after the reflected waves from the damping beach arrived at the cylinder. At the same time, the IMU drifted from the middle of the ice floe to the edge due to overwash and was removed before it fell into the water.

**TABLE 2:** PRESCRIBED EXPERIMENTAL PARAMETERS (OPEN-WATER SCENARIO: TEST SERIES #5000, ICE-INFESTED WATERS: TEST SERIES #4000)

| Run ID (Series #5000 / #4000) | $T$ [s] | $H$ [m] | $\sqrt{ka}$ |
|---|---|---|---|
| #5110 / #4110 | 2.0 | 0.025 | 0.5886 |
| #5120 / #4120 | 1.8 | 0.025 | 0.6512 |
| #5130 / #4130 | 1.6 | 0.025 | 0.7314 |
| #5140 / #4140 | 1.5 | 0.025 | 0.7799 |
| #5210 / #4210 | 2.0 | 0.050 | 0.5886 |
| #5220 / #4220 | 1.8 | 0.050 | 0.6512 |
| #5230 / #4230 | 1.6 | 0.050 | 0.7314 |
| #5240 / #4240 | 1.5 | 0.050 | 0.7799 |
| #5310 / #4310 | 2.0 | 0.075 | 0.5886 |
| #5320 / #4320 | 1.8 | 0.075 | 0.6512 |
| #5330 / #4330 | 1.6 | 0.075 | 0.7314 |
| #5340 / #4340 | 1.5 | 0.075 | 0.7799 |
| #5430 / #4430 | 1.6 | 0.100 | 0.7314 |

The majority of these tested wave conditions fall within Stoke's second-order wave theory domain ($H > 0.025\,m$), whereas the rest satisfy linear wave assumption (see Fig. 4). When classifying waves in terms of water depth ($d$) and wavelength ($\lambda$), the experimental waves are within the domain of intermediate depth waves ($T = 2\,s$) and deep water waves (wave periods $T < 2\,s$).

Additionally, note that the only differences in terms of setup between test series #4000 (ice-infested water) and #5000 (open water) are whether the basin was partially covered by ice floes and whether the IMU was deployed or not.

## 3. DATA ANALYSIS METHODS

Appropriate data analysis techniques are necessary to interpret data properly. Here, several methods to obtain the amplitudes of wave and wave loads are described in brevity.

Prony method [18] and dynamic mode decomposition (DMD, [19, 20]) decompose a time series into a number of damped complex exponential constituents. This decomposition takes the form:

$$\eta = \sum_{q=1}^{r} \eta_q^a \exp(\alpha_q t) \exp(i(\omega_q t + \theta_q)) \tag{1}$$

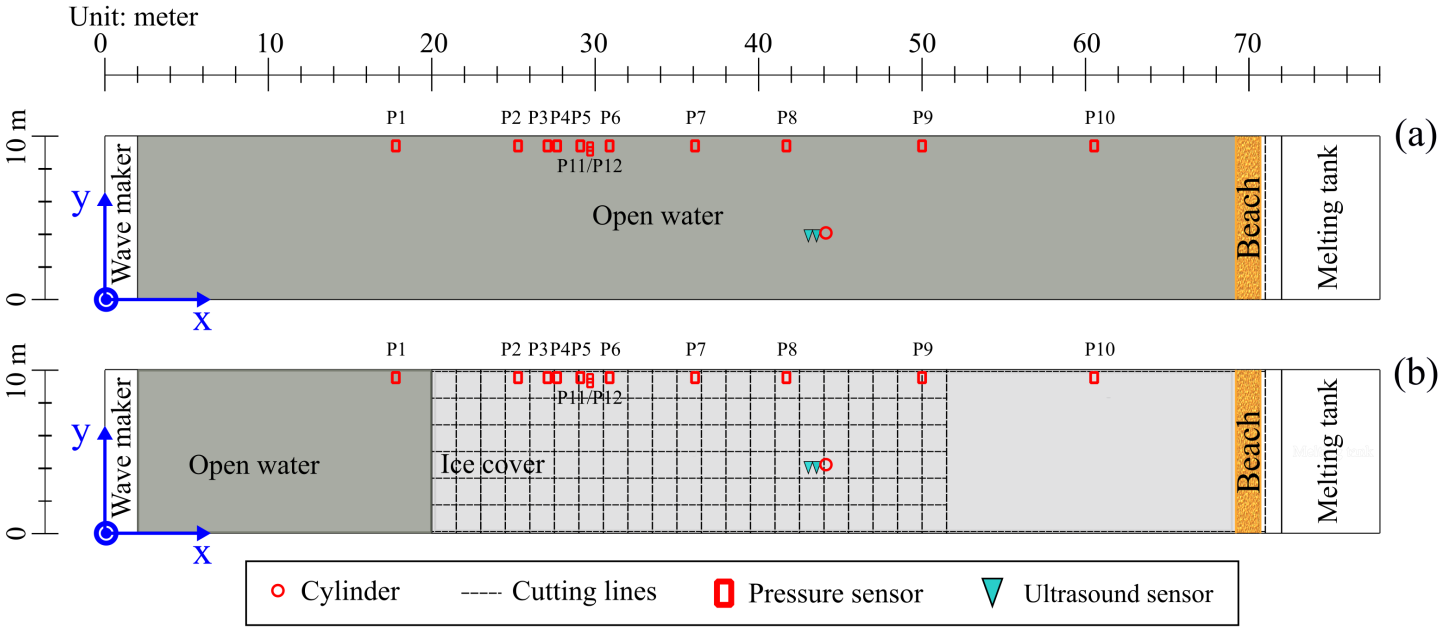


**FIGURE 1:** SKETCH OF THE LS-WICE EXPERIMENTAL SETUP (ADAPTED FROM Ref. [16]). (a) TEST SERIES #5000. (b) TEST SERIES #4000. NOTE THAT THE POSITIONS OF THE CIRCULAR CYLINDER AND VARIOUS SENSORS WERE IDENTICAL BETWEEN THESE TWO TEST SERIES.

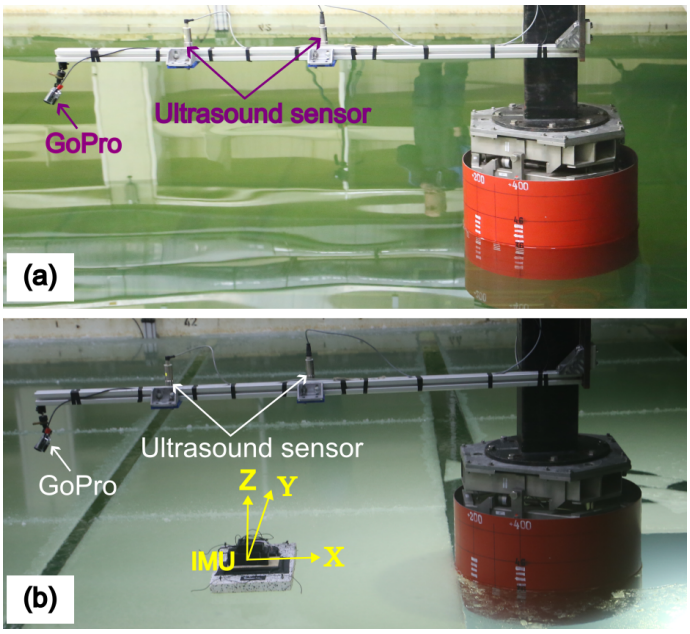


**FIGURE 2:** PHOTOS DISPLAYING THE ARRANGEMENT OF SENSORS IN THE NEIGHBORHOOD OF THE HOLLOW CYLINDER. (a) TEST SERIES #5000. (b) TEST SERIES #4000.

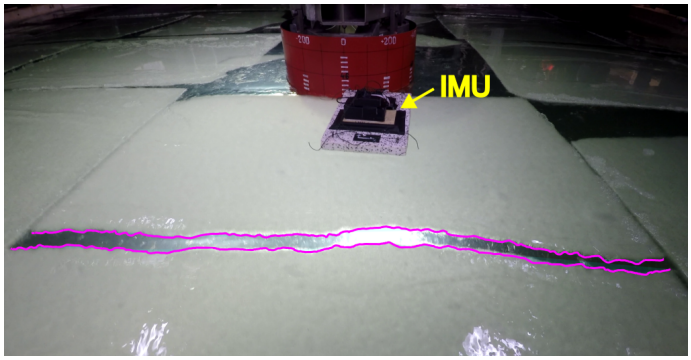


**FIGURE 3:** STILL IMAGE FROM THE VIDEO TAKEN BY THE GO-PRO CAMERA SHOWING THE ICE FLOE NEXT TO THE CYLINDER WAS BROKEN UNDER WAVE ACTIONS AND COLLISIONS WITH THE CYLINDER DURING TEST RUN #4330 ($T$ = 1.6 s, $H$ = 0.075 m). MAGENTA LINES HIGHLIGHT THE EDGES OF THE CRACK.

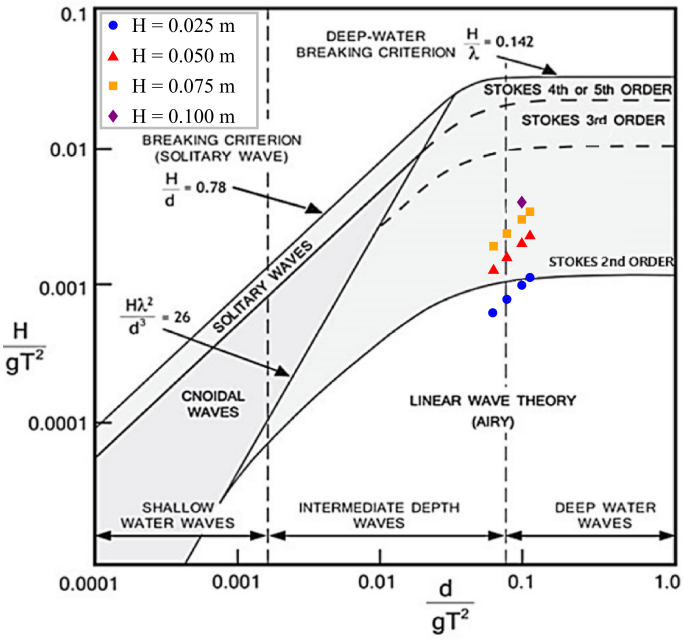


**FIGURE 4:** VALIDITY RANGE OF DIFFERENT WAVE THEORIES (ADAPTED FROM Ref. [17]). MARKERS OF VARIOUS COLORS DENOTE WAVE CONDITIONS EXPERIMENTED.

where $\eta^a$, $\alpha$, $\omega$, and $\theta$ are amplitude, decay rate, radian frequency, and phase, respectively.

The optimal number ($r$) of the complex components to reconstruct the original signal are determined by truncated singular value decomposition method [21] for the Prony method and optimal hard thresholding method [22] for DMD.

Amplitudes of the incoming wave and wave loads corresponding to wave frequency are estimated by peak analysis that is carried out on the time series reconstructed by using only the wave-frequency component.

Another method is to denoise the signals first by using the Tikhonov regularization method as proposed by Ref. [23], and then perform peak analysis on the smoothed signals. We refer to this method as Tik-peak henceforth.

We also apply the fast Fourier transform (FFT) in conjunction with selecting a section of time series with zero values and periodic conditions at both ends to estimate amplitude (see Ref. [23] and Fig. 14 in Appendix A). This way of choosing time history contributes to mitigating spectral leakage. When isolating a part of a time series with the aforementioned characteristics is very challenging, a flat-top weighted window that is most suitable for amplitude estimation is employed before using FFT to alleviate the effect of leakage on determining amplitude [24–26]. Thereafter, a coefficient of this window is utilized to rectify the effect of windowing on the estimated amplitude.

The last approach to extract wave loads in correspondence with wave frequency is Singular Spectrum analysis (SSA) [12, 13]. This approach is based on the time-delayed method and singular value decomposition [27].

## 4. WAVE AMPLITUDE

Wave measurements in any wave/ice tank are subject to reflected waves from damping beach and structures installed inside [14, 28]. Generated waves also evolve in the traveling direction [29].

Here we investigate the progressive change of waves along the ice basin and quantify the effect of the circular cylinder on the waves measured at pressure sensor P8. The reason we especially focus on this sensor is that the waves at P8 may serve as the incident waves that directly inflict upon the cylinder in ice-infested water due to: (1) its proximity to the cylinder (Fig. 1); (2) waves did not damp appreciably in the interior part of the ice cover in comparison to the domain near the leading edge under the laboratory setting of LS-WICE [15]; (3) inapplicability of measurements at other pressure sensors because wave attenuates in ice field. To justify utilizing the wave data collected from P8, we will show that the cylinder did not influence significantly the wave field. However, one assumption has to be made, i.e., the characteristics of the wave reflected from the cylinder were unchanging between the open-water case and the ice-covered scenario.

To achieve the aforementioned two objectives, we use the time series of wave elevations obtained with pressure sensors P1 - P6 that are free from reflections from the cylinder, hence those from absorbing beach, as well as the time history of wave measurements at sensor P8 that was not contaminated by reflected waves due to beach. Measurements from different sets of pressure sensors are selected for test runs with distinct wave periods to ensure sufficiently long quasi-steady time series before reflected waves reached each sensor (as an example, see Fig. 14 in Appendix A). Time series from collocated sensors P11 and P12 are skipped as their connection to the data acquisition system was broken during the experiment.

### 4.1 Wave amplitudes in open water

Experimental wave amplitudes determined by a variety of methods are shown in Figs. 5 and 6. All four methods yield very similar estimates. Wave amplitudes at sensors P1 - P3 agree well with those prescribed ones (absolute normalized difference is within 10.1%, see Fig. 7), while the remainder generally is higher. Notably, wave amplitudes at P8 are close to the targeted ones for most test runs. The exceptions are the test runs with wave period 1.5 $s$ and targeted wave amplitudes 0.0125 $m$ and 0.025 $m$ (Fig. 6d).

Figure 7 shows the absolute normalized difference (ND) of amplitude estimated by the Tik-peak method relative to the prescribed wave amplitude. Results from the other methods are not presented here because of their similar performance as the Tik-peak method (see Figs. 5 - 6). Additionally, ND for sensor P6 is ruled out as there are only three estimates from this device (Fig. 5 - 6). As seen in Fig. 7, ND tends to increase in the wave propagation direction, from 10% to 14.2% in terms of maximum values for sensors P2 - P5. This rise can be attributed to the influence of vortices, induced by the oscillating motion of waves and shed from these sensors, on the neighboring pressure sensors. This is substantiated by that these sensors are close to each other in space, see Fig. 1 and Figs. 5 - 6, with the maximum separation between the adjacent pairs to be 60% of the smallest wavelength.

In contrast, sensor P1 is far from the other pressure sensors with a distance to its closest nearby sensor P2, 1.3 times the longest waves. ND corresponding to P1 is within 5.7%. *After accounting for the uncertainty of wave measurements, the targeted wave amplitude should be used when determining wave loads on the cylinder under open water conditions*.

As mentioned at the beginning of this section, the time series of waves from sensor P8 used in the analysis include the reflection from the cylinder, whereas the other pressure sensors do not. Considering the interference between sensors P2 - P5, we quantify the effect of reflected waves on measurements from P8 by comparing ND associated with P1 and P8 only. When excluding the outlier and the maximum, which relates to the two test runs having $T = 1.5\,s$ with obvious deviation from the targeted wave amplitude as illustrated in Fig. 6d, ND is within 15.1% for P8. Hence, the reflection from the cylinder comprises approximately 10% (15.1% − 5% (P1)) of wave amplitude estimated from the measurement for most test runs. Consequently, it is reasonable to use wave measurements at sensor P8 to represent the incoming waves that induce wave loads on the cylinder in an ice-covered case when wave period $T > 1.5\,s$.

A recent laboratory study [28] reported a pronounced discrepancy of as much as 30%, particularly for waves with small wavelength, of measured wave amplitude between the wave probes at the sidewalls next to a cylinder and one wave probe situated far away in the up-wave direction. A similar significant amount of deviation is observed herein as well, see the outlier at P8 corresponding to the shortest waves ($T = 1.5\,s$) tested herein and the ND for P1 in Fig. 7. In Ref. [28], the cylinder deployed is an analogous vertical, open-bottom, semi-submerged, circular structure but with baffles. Therein, the breadth of ocean basin over the external diameter of the cylinder is 13.13, which is similar to 14.64 for the present study.

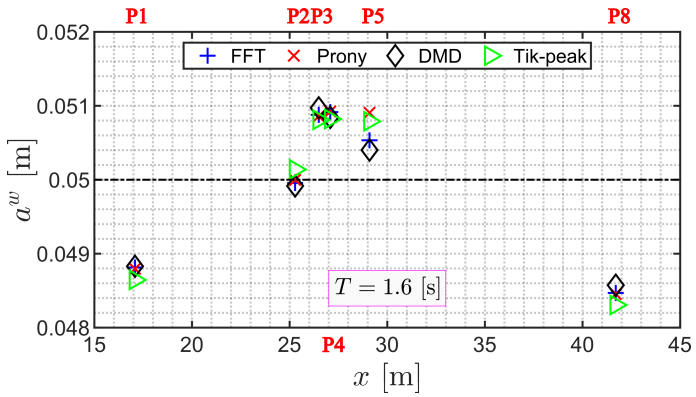


**FIGURE 5:** WAVE AMPLITUDES ESTIMATED BY VARIOUS METHODS USING THE MEASUREMENTS OF WAVE ELEVATIONS TAKEN AT PRESSURE SENSORS P1 - P5 AND P8 (OPEN WATER, TEST RUN #5430, $T$ = 1.6 s, $H$ = 0.100 m).

### 4.2 Wave amplitudes in ice-infested water

Waves attenuate and lengthen or shorten as they penetrate into an ice field [30, 31]. Here, we concentrate on wave attenuation.

As an example, Fig. 8 displays the quasi-steady part of wave measurements taken at pressure sensor P8 for test run #5330 ($T = 1.6\,s$, $H = 0.075\,m$) and its ice-covered counterpart. As can be seen clearly, wave amplitude decreases from around 0.039 $m$ in open water (Fig. 8a) to nearly 0.02 $m$ in ice-infested water (Fig. 8b). Moreover, Prony successfully extracts the wave-frequency component and Tikhonov smooths out high-frequency oscillations. Differences in the signals obtained with these two methods are barely noticeable. DMD produces a result that is in agreement with that from Prony, but not shown here to avoid clutter.

Figure 9 summarizes the wave amplitudes at sensor P8 estimated by FFT, Prony, DMD, and Tik-peak in comparison with the estimations given in Ref. [11]. Concordant with the results for the open-water case shown in subsection 4.1, these four methods give close estimates of wave amplitude. However, these differ from Ref. [11] in six out of 11 test runs (see those markered by dashed-line black boxes in Fig. 9a). In LS-WICE experiments, the length of waves in ice differs from the open-water one by up to 5% (see Ref. [32] and reference therein). This results in a maximum of 3.6% difference of wave amplitude in ice from the open-water value during converting the measured underwater pressure to wave elevation, hence wave amplitude. Fig. 9b depicts that the evident deviations from Ref. [11] persist for four of six test runs even after accounting for wavelength change by multiplying the quantified amplitude from the four methods by a conservative value of 1.05 (those highlighted by dashed-line black boxes in Fig. 9b).

Here, wave amplitude estimates associated with open-water wavelength are adopted for further analysis. There are two reasons: (1) wave in an ice field continuously evolves, i.e. both its amplitude and length; any estimate of wavelength by wave measurements from pairs of pressure sensors is thereby an average along wave propagation direction; (2) the averaged wavelength determined from measurements deviates within 5% from the open-water one as mentioned above.

Since the four methods applied here yield very similar wave amplitudes for both open-water and ice-covered cases, we will only use our wave amplitude results in icy water for corresponding wave load comparison with open-water situation.

Additionally, the ice cover here is shown to be a low-pass filter (Fig. 9), i.e. wave energy reduces more with the increase of wave frequency (see Table 2 for the values of $\sqrt{ka}$ and wave period $T$). This reflects the observations made in in-situ field experiments (see Ref. [31] and references therein).

## 5. EXPERIMENTALLY DETERMINED WAVE LOADS

Wave loads on the hollow cylinder, situated in open water and ice-infested water respectively, are compared here.

### 5.1 An illustrative case

As an example, various wave load amplitude estimation approaches are applied to test run #5330 ($T = 1.6\,s$, $H = 0.075\,m$) and its corresponding test run #4330 under icy condition.

Figure 10 shows the time history of the loads on the cylinder in open and icy waters. Figure 10a illustrates that the denoised wave loads time series obtained by Tikhonov matches closely with

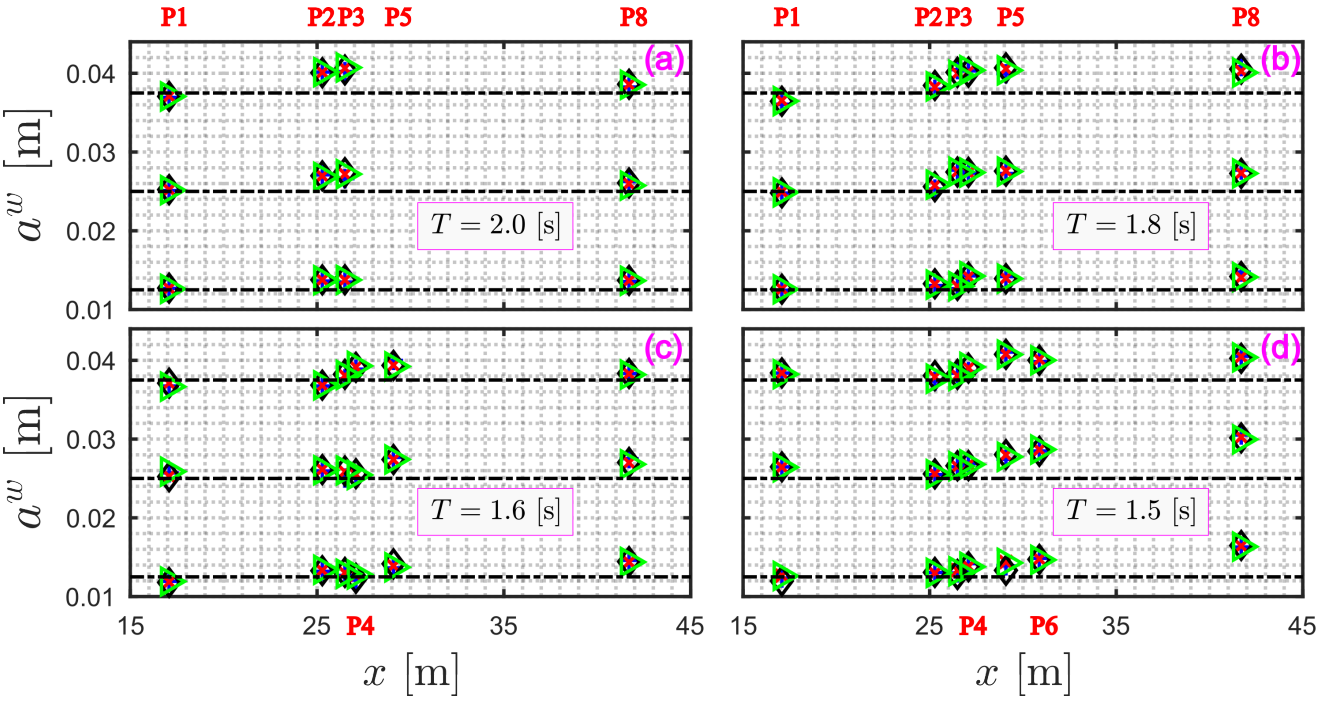


**FIGURE 6:** VARIATION OF WAVE AMPLITUDES IN THE STREAMWISE DIRECTION IN OPEN WATER. BLUE PLUSS SIGN: FFT. RED CROSS: PRONY. BLACK DIAMOND: DMD. GREEN RIGHT-POINTING TRIANGLE: TIK-PEAK. BLACK DASH-DOTTED LINES REPRESENT THE TARGETED WAVE AMPLITUDE THAT VARIES FROM 0.0125 m TO 0.0375 m WITH A CONSTANT INCREMENT OF 0.0125 m. (a) TEST RUNS #5110, #5210 AND #5310. (b) TEST RUNS #5120, #5220 AND #5320. (c) TEST RUNS #5130, #5230 AND #5330. (d) TEST RUNS #5140, #5240 AND #5340. NOTE THAT THE TEST RUNS MENTIONED IN THE CAPTION ARE ARRANGED IN THE ASCENDING ORDER OF PRESCRIBED WAVE AMPLITUDE.

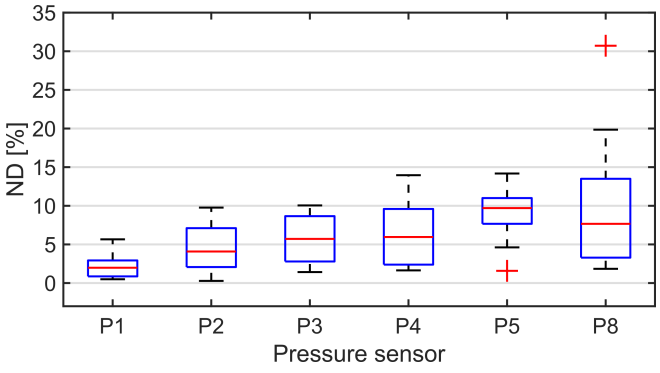


**FIGURE 7:** ABSOLUTE NORMALIZED DIFFERENCE (ND) OF MEASURED WAVE AMPLITUDES RELATIVE TO THOSE PRESCRIBED ONES AT PRESSURE SENSORS P1 - P5 AND P8 (OPEN WATER, TEST SERIES #5000).

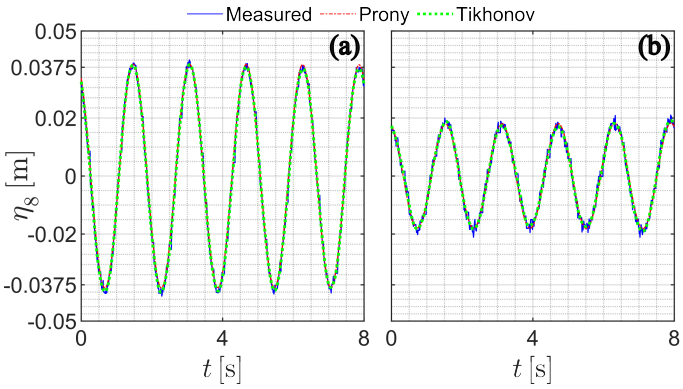


**FIGURE 8:** COMPARISON OF WAVE ELEVATIONS MEASURED AT PRESSURE SENSOR P8. (a) OPEN-WATER CASE (TEST RUN #5330, $T$ = 1.6 s, $H$ = 0.075 m). (b) ICE-INFESTED SCENARIO (TEST RUN #4330, $T$ = 1.6 s, $H$ = 0.075 m).

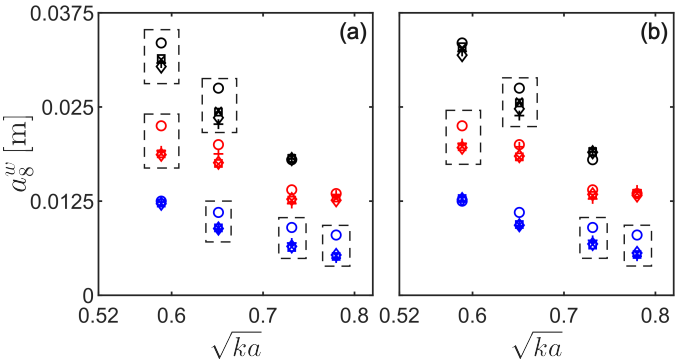


**FIGURE 9:** WAVE AMPLITUDES IN ICY WATERS AT P8 (TEST SERIES #4000). CIRCLE: Ref. [11]. PLUS SIGN: FFT. CROSS: PRONY. DIAMOND: DMD. SQUARE: TIK-PEAK. BLACK: $H$ = 0.075 m. RED: $H$ = 0.050 m. BLUE: $H$ = 0.025 m. DASHED-LINE RECTANGLE EMPHASIZES THE DIFFERENCES FROM Ref. [11]. (a) USE WAVELENGTH IN OPEN WATER. (b) CONSIDER THE EFFECT OF ICE ON WAVELENGTH, THUS ESTIMATING WAVE AMPLITUDE BY MAGNIFYING THOSE IN (a) BY 1.05.

the measured one. However, high-frequency noise is eliminated by Tikhonov as demonstrated by Fig. 10b.

From Fig. 10c, we observe that the cylinder experienced ice-induced resonant response (high-frequency oscillations). This resulted from the waves drove the upstream ice floe to collide with the cylinder. As for the ice floe next to the cylinder in the down-wave direction, it did not bump to the cylinder because of the large gap between them (see Fig. 2b). As seen in Fig. 10c, the impact load from ice is much higher than the wave loads identified by using Prony and DMD. The wave loads extracted appear reasonable because they follow the sinusoidal trend well. Especially, the wave-frequency component in the sinusoidal-like load measurements between 4 $s$ and 6.5 $s$, when the eigen response of the cylinder was almost absent, is captured well by Prony and DMD.

Figure 10 also illustrates that wave loads decrease markedly from around 70 $N$ under open-water condition (Fig. 10a) to nearly 60 $N$ in ice-infested waters (Fig. 10c).

The rest of force time history from test run #4330 ($T$ = 1.6 $s$, $H$ = 0.075 $m$) selected for analysis is presented in Fig. 11a. Similar to Fig. 10c, the identified wave loads by Prony trace the sinusoidal trend well, which is the case for SSA as well. Analogous to the load time series between 4 $s$ and 6.5 $s$ in Fig. 10c, the inline force time series between 11 $s$ and 13.2 $s$ was barely affected by the resonant vibrations of the cylinder. Prony and SSA successfully extract the wave loads from this part of the signal. The noticeable disparity in identified wave loads by these two methods exists only near the boundary (Fig. 11b). Resultant wave loads obtained with DMD are extremely similar to those found by SSA and Prony. Thus, corresponding results from using DMD are not shown here to prevent clutter.

### 5.2 Wave loads for all experimental conditions

We compare our identified wave loads using SSA, Prony, DMD, and FFT to the results given in Ref. [11] for the ice-covered test series #4000 in Fig. 12. There are three cases highlighted by the dashed-line rectangles where extracted wave loads from Ref. [11] differ distinctly from our results. This discrepancy is most likely the result of spectral leakage when applying FFT without using a smoothing window in Ref. [11].

Since all four methods employed here produce very similar results, we only use the wave loads in icy water extracted by Prony to compare with the open-water scenario.

As for the ice-free water case, the load signals resemble sinusoids (e.g. Fig. 10a), and corresponding wave load amplitudes are hence found by using Tik-peak. The reason is that this method along with FFT, Prony, and DMD gives very similar results when sinusoid-like signals are analyzed (Figs. 5 - 6 and Figs. 8 - 9).

As an additional remark on these methods, Prony is superior to DMD as sometimes re-selecting a quasi-steady part of the whole signal is required for DMD to successfully identify wave loads. In contrast, SSA is cumbersome to utilize but does provide intuition in the various modes that compose signals. Concerning estimating amplitudes, FFT combined with flat top weighted window is most efficient. However, this method fails to show precisely the temporal variation of wave-frequency components due to windowing. Regarding Tik-peak, it is only applicable to quasi-periodic signals. Therefore, Prony is recommended to be used to analyze both wave and load measurements.

To reveal how wave attenuation affects the wave loads on the cylinder, we graph the ratio of wave loads in icy water over those in open water versus the relevant ratio of wave amplitude in Fig. 13. It can be seen that wave loads decrease together with wave amplitude in ice-infested water when $T = 2\,s$. In one of the test runs when $T = 2\,s$, the load increases even though wave amplitude decreases. For the other test runs, the ratio of wave loads varies between 0.7 and 0.9 as that of wave amplitude reduces from 0.72 to 0.41. This implies that the wave-ice-structure interaction is complex, and wave loads do not decrease linearly with wave amplitude in icy water. However, the damping of waves in ice field does lead to the reduction of wave loads on the cylinder. This is consistent with the findings of another experimental study [9], in which the more attenuation of waves in higher concentrations of ice floes results in a further decrease of wave-ice loads.

## 6. CONCLUSION

This paper investigates experimentally the inline wave loads on an open-bottom, vertical, thin-walled circular cylinder in open water and a broken saline ice field. This is the first systematic comparative study on wave loads exerted on a hollow cylinder under the aforementioned environmental conditions in a laboratory.

A variety of data analysis techniques, such as FFT, Prony, DMD, Tik-peak, and the method SSA introduced to the Arctic engineering community, are utilized to ensure the high-quality estimates of wave amplitude and the amplitudes of wave loads. Estimates obtained using these methods closely match each other. Considering efficiency and stability in performance, we suggest the Prony method to analyze wave and load signals.

The analysis of the experimental data using the aforementioned techniques suggests that the wave increasingly damps out with wave frequency, as far as measurements from a sensor in close vicinity of the cylinder are concerned.

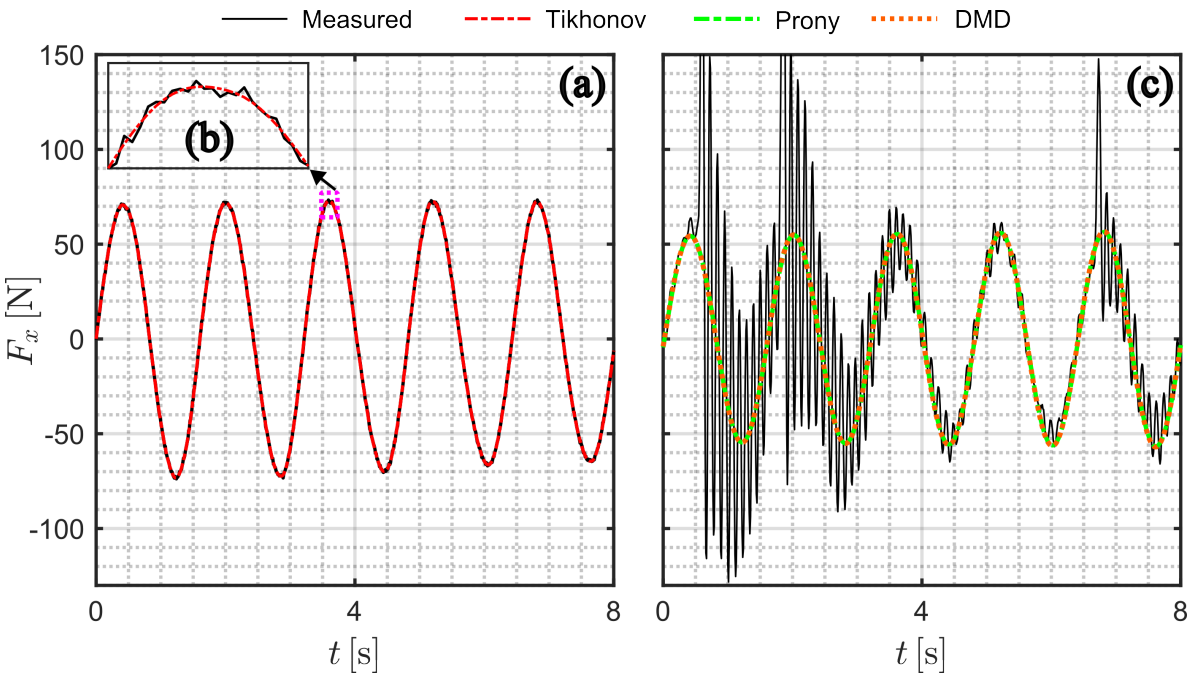


**FIGURE 10:** COMPARE WAVE LOADS. (a) OPEN-WATER CASE (TEST RUN #5330, $T$ = 1.6 s, $H$ = 0.075 m). (b) INSET IS A ZOOMED-IN VIEW OF THE MAGENTA DASHED-LINE BOX IN (a) AND STRESSES THAT TIKHONOV REMOVES HIGH-FREQUENCY NOISE. (c) ICY-WATER CASE (TEST RUN #4330, $T$ = 1.6 s, $H$ = 0.075 m). NOTE THAT PANEL (a) ONLY INCLUDES MEASURED WAVE LOADS AND THE RESULTS FROM TIKHONOV TO CIRCUMVENT CLUTTER, AND TIKHONOV IS NOT USED TO IDENTIFY WAVE LOADS IN PANEL (c).

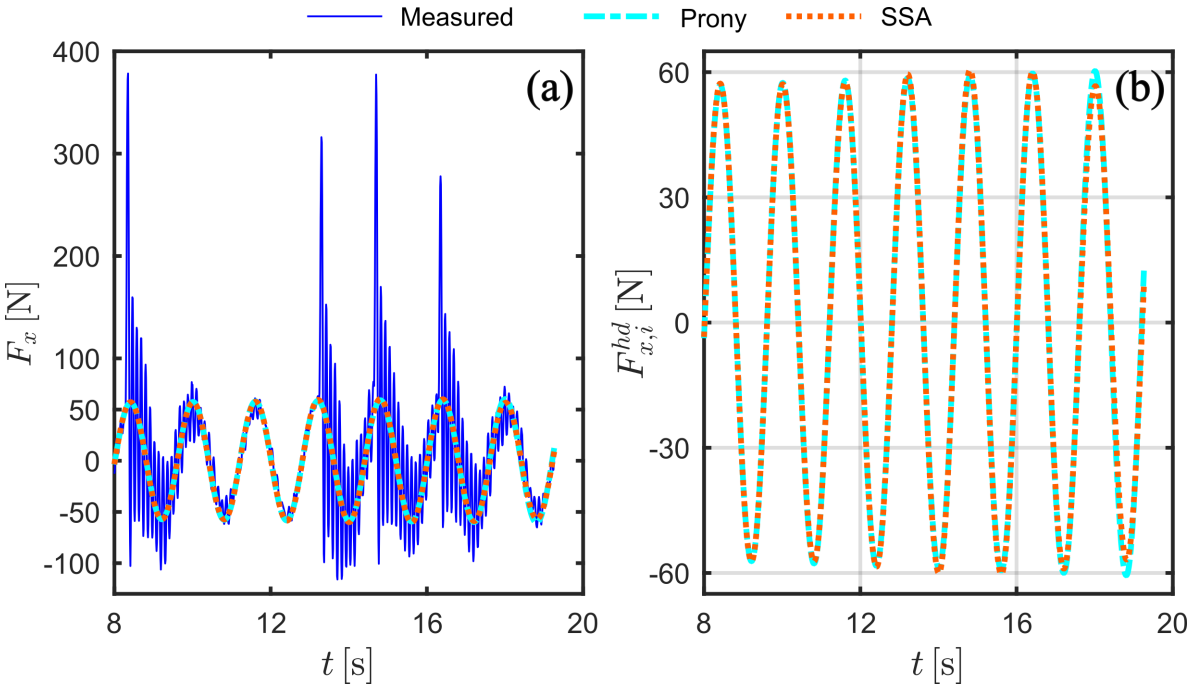


**FIGURE 11:** IDENTIFY WAVE LOADS FOR TEST RUN #4330 ($T$ = 1.6 s, $H$ = 0.075 m) UNDER ICE-COVERED CONDITION. (a) MEASURED LOADS IN SURGE DIRECTION. (b) EXTRACTED WAVE LOADS. SUBSCRIPT $i$ IN $F^{hd}_{x,i}$ DENOTES ICE.

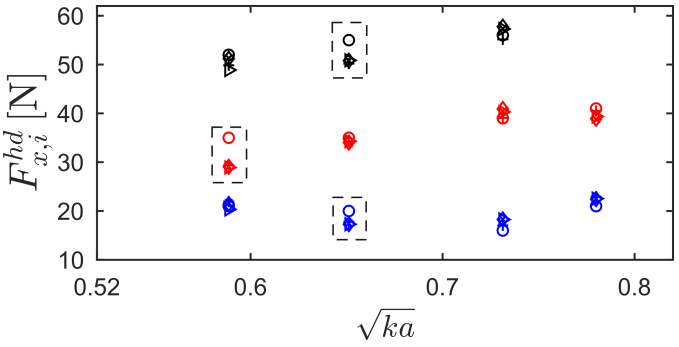


**FIGURE 12:** EXTRACTED WAVE LOADS FOR ICE-COVERED SCENARIO (TEST SERIES #4000). CIRCLE: Ref. [11]. PLUS SIGN: FFT. DIAMOND: DMD. RIGHT-POINTING TRIANGLE: SSA. BLACK: $H$ = 0.075 m. RED: $H$ = 0.050 m. BLUE: $H$ = 0.025 m. BLACK DASHED-LINE RECTANGLE HIGHLIGHTS DEVIATIONS FROM Ref. [11].

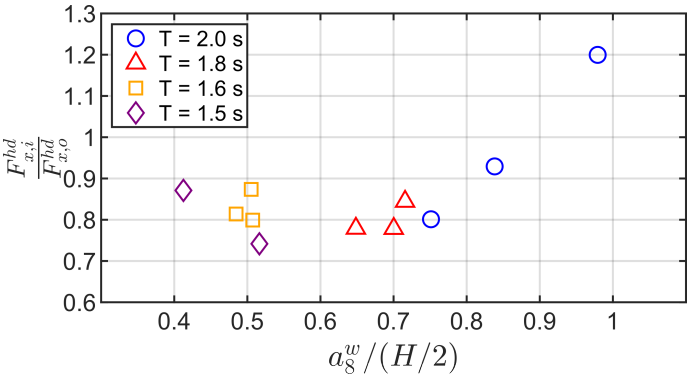


**FIGURE 13:** RATIO OF THE WAVE LOADS UNDER ICY-WATER CONDITIONS OVER THOSE IN OPEN WATER AGAINST THE CORRESPONDING WAVE AMPLITUDE RATIO. SUBSCRIPTS ***o*** AND ***i*** REPRESENT OPEN WATER AND ICE, RESPECTIVELY.

When the analysis of wave amplitudes is combined with the analysis of wave loads by using the extensive dataset presented, we affirm that wave attenuation generally results in a decrease in wave loads.

## ACKNOWLEDGMENTS

The leading author and J. Sawamura would like to acknowledge the support provided by the Japanese Ministry of Education, Culture, Sports, Science, and Technology through the Arctic Challenge for Sustainability II (ArCS II) Project under Grant No. JPMXD1420318865. The experiments demonstrated in this study were financed by the European Community's Horizon 2020 Programme through a grant to the budget of the Integrated Infrastructure Initiative HYDRALAB+, contract no. 654110. E. D. Gedikli would like to acknowledge the support received from the National Science Foundation Navigating the New Arctic Big Idea under Grant No. 2127095. The first author is also very grateful for the discussions with Wenjun Lu from the Norwegian University of Science and Technology.

## REFERENCES

[1] N. Adomaitis, G. Fouche. "Norway plans to offer record number of Arctic oil, gas exploration blocks." Reuters (2023). Accessed December 16, 2023, URL https://www.reuters.com/business/energy/norway-offers-up-92-new-oil-gas-exploration-blocks-2023-01-24/.

[2] M. Cecchinato. "Boosting offshore wind energy in the Baltic Sea." Wind Europe (2019). Accessed December 16, 2023, URL https://windeurope.org/wp-content/uploads/files/about-wind/reports/WindEurope-Boosting-offshore-wind.pdf.

[3] M. Christensen, M. Georgati, J.J. Arsanjani. "A risk-based approach for determining the future potential of commercial shipping in the Arctic." *Journal of Marine Engineering & Technology* Vol. 21 No. 2 (2022): pp. 82–99.

[4] G.J. Peel, E.D. Gedikli, H. Hendrikse. "Navigating Arctic Waters: A Summary of Ship Activities and Ice-Ship Interactions in Alaskan Waters." *Proceedings of the 27th International Conference on Port and Ocean Engineering under Arctic Conditions*. Glasgow, UK, 2023. POAC.

[5] O.T. Gudmestad. "Recent Norwegian Research Relevant to Evacuation, Search and Rescue under Arctic Conditions." *IOP Conference Series: Earth and Environmental Science*, Vol. 987. 1: p. 012005. 2022. IOP Publishing.

[6] M. Bjerkås, T.S. Nord. "Ice action on Swedish lighthouses revisited." *Proceedings of The 23rd International Symposium on Ice*. Ann Arbor, Michigan, USA, 2016. The International Association for Hydro-Environment Engineering and Research.

[7] T.S. Nord, E. Lourens, O. Øiseth, A. Metrikine. "Model-based force and state estimation in experimental ice-induced vibrations by means of Kalman filtering." *Cold Regions Science and Technology* Vol. 111 (2015): pp. 13–26.

[8] T.C. Hammer, T. Willems, H. Hendrikse. "Dynamic ice loads for offshore wind support structure design." *Marine Structures* Vol. 87 (2023): p. 103335.

[9] S. Mintu, D. Molyneux. "Experimental study of combined wave and ice loads on a fixed offshore structure." *International Conference on Offshore Mechanics and Arctic Engineering*, Vol. 85178: p. V007T07A010. 2021. American Society of Mechanical Engineers.

[10] J. Sawamura, K. Imaki, T. Shiraishi, H. Senga. "Ice Resistance test of a ship using synthetic ice in small pack ice floes and wave interactions." *ISOPE International Ocean and Polar Engineering Conference*. 2018. ISOPE.

[11] A. Tsarau, S. Sukhorukov, A. Herman, K. Evers, S. Løset. "Loads on Structure and Waves in Ice (LS-WICE) project, Part 3: Ice-structure interaction under wave conditions." *Proceedings of the International Conference on Port and Ocean Engineering Under Arctic Conditions*. Pusan, Korea, June 11–16, 2017. Korea Maritime & Ocean University.

[12] N. Golyandina, A. Korobeynikov, A. Zhigljavsky. *Singular spectrum analysis with R*. Springer (2018).

[13] N. Golyandina, A. Zhigljavsky. *Singular Spectrum Analysis for Time Series*. Springer Berlin Heidelberg (2020).

[14] S. Cheng, A. Tsarau, K. Evers, H.H. Shen. "Floe size effect on gravity wave propagation through ice covers." *Journal of Geophysical Research: Oceans* Vol. 124 No. 1 (2019): pp. 320–334.

[15] A. Herman, S. Cheng, H.H. Shen. "Wave energy attenuation in fields of colliding ice floes–Part 2: A laboratory case study." *The Cryosphere* Vol. 13 No. 11 (2019): pp. 2901–2914.

[16] H. Li, E.D. Gedikli, R. Lubbad. "Laboratory study of wave-induced flexural motion of ice floes." *Cold Regions Science and Technology* Vol. 182 (2021): p. 103208.

[17] B. Le Méhauté. "An introduction to water waves." *An introduction to hydrodynamics and water waves* (1976): pp. 197–211.

[18] S.J. Hu, W. Yang, H. Li. "Signal decomposition and reconstruction using complex exponential models." *Mechanical Systems and Signal Processing* Vol. 40 No. 2 (2013): pp. 421–438.

[19] P.J. Schmid. "Dynamic mode decomposition of numerical and experimental data." *Journal of fluid mechanics* Vol. 656 (2010): pp. 5–28.

[20] J.H. Tu, C.W. Rowley, D.M. Luchtenburg, S.L. Brunton, J.N. Kutz. "On dynamic mode decomposition: theory and applications." *Journal of Computational Dynamics* Vol. 1 (2014): pp. 391–421.

[21] J.L. Mueller, S. Siltanen. *Linear and nonlinear inverse problems with practical applications*. SIAM (2012).

[22] M. Gavish, D.L. Donoho. "The optimal hard threshold for singular values is $4/\sqrt{3}$." *IEEE Transactions on Information Theory* Vol. 60 No. 8 (2014): pp. 5040–5053.

[23] H. Li, E.D. Gedikli, R. Lubbad. "Systematic investigation of data analysis methods in wave-ice interaction problem." *Proceedings of The 25th International Symposium on Ice*. Trondheim, Norway, November 23–25, 2020. The International Association for Hydro-Environment Engineering and Research.

[24] G. D'Antona, A. Ferrero. *Digital signal processing for measurement systems: theory and applications*. Springer Science & Business Media (2005).

[25] Simcenter Testing Knowledge Base Community. "Digital signal processing knowledge booklet - testing knowledge base compilation." SIEMENS (2019). Accessed August 05, 2023, URL https://view.highspot.com/viewer/5d41817278e87d04a9ed430e.

[26] UMass Lowell Structural Dynamics & Acoustic Systems Laboratory. "Windows and leakage brief overview." (2007). Accessed August 18, 2023, URL https://www.uml.edu/docs/Windows-Leakage%5Ftcm18-191248.pdf.

[27] D.S. Broomhead, G.P. King. "Extracting qualitative dynamics from experimental data." *Physica D: Nonlinear Phenomena* Vol. 20 No. 2-3 (1986): pp. 217–236.

[28] M. Moreau, T. Kristiansen, B. Ommani, B. Molin. "An upright bottomless vertical cylinder with baffles floating in waves." *Applied Ocean Research* Vol. 119 (2022): p. 102934.

[29] M. Huseby, J. Grue. "An experimental investigation of higher-harmonic wave forces on a vertical cylinder." *Journal of fluid Mechanics* Vol. 414 (2000): pp. 75–103.

[30] M.H. Meylan, L.G. Bennetts, J.E.M. Mosig, W.E. Rogers, M.J. Doble, M.A. Peter. "Dispersion relations, power laws, and energy loss for waves in the marginal ice zone." *Journal of Geophysical Research: Oceans* Vol. 123 No. 5 (2018): pp. 3322–3335.

[31] H.H. Shen. "Wave-in-ice: theoretical bases and field observations." *Philosophical Transactions of the Royal Society A* Vol. 380 No. 2235 (2022): p. 20210254.

[32] A. Herman, K. Evers, N. Reimer. "Floe-size distributions in laboratory ice broken by waves." *The Cryosphere* Vol. 12 No. 2 (2018): pp. 685–699.

## APPENDIX A. SELECTING NON-CONTAMINATED QUASI-STEADY WAVE MEASUREMENTS

Figure 14 illustrates how quasi-steady wave measurements, which are free from reflected waves, are chosen.

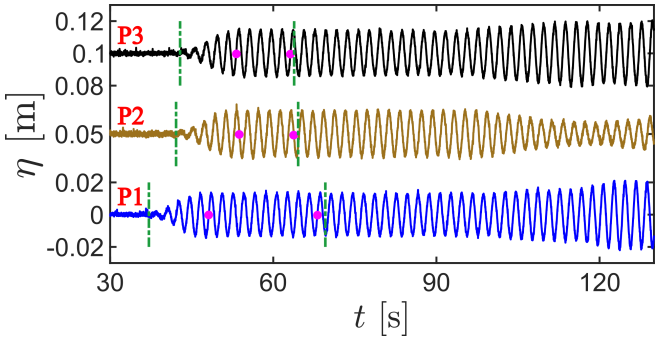


**FIGURE 14:** DEMONSTRATION OF CHOOSING QUASI-STEADY MEASURED WAVE ELEVATIONS WITHOUT REFLECTIONS (TEST RUN #5110, $T$ = 2.0 s, $H$ = 0.025 m). EACH PAIR OF GREEN DASH-DOTTED LINES INDICATES THE TIME INTERVAL BETWEEN GENERATED WAVES ARRIVING AT EACH SENSOR AND THE WAVES REFLECTED BY THE CYLINDER JUST BEFORE REACHING THOSE SENSORS. EACH PAIR OF MAGENTA DOTS HIGHLIGHTS THE QUASI-STEADY TIME SERIES WITH ZERO PERIODIC BOUNDARY CHOSEN FOR ANALYSIS. WAVE MEASUREMENTS FROM SENSORS P2 AND P3 ARE SHIFTED UP WITH 0.05 m AND 0.10 m RESPECTIVELY TO AID VISUALIZATIONS.